The Multimessenger Chakra of Blazar Jets
Proceedings IAU Symposium No. 375, 2023
I. Liodakis, M. F. Aller, H. Krawczynski, A. Lähteenmäki & T. J. Pearson, eds.
doi:10.1017/S1743921323000637

Effect of Inverse Compton Cooling on Relativistic Particles Accelerated at Shear Boundary Layers in Relativistic Jets

Tej Chand and Markus Böttcher

Centre for Space Research, North-West University, Potchefstroom, 2520, South Africa
emails: chandtej11@gmail.com, Markus.Bottcher@nwu.ac.za

Abstract. Recent theoretical considerations and observational evidence evince the spine-sheath morphology of relativistic jets emitted from active galactic nuclei (AGNs) or gamma-ray bursts (GRBs). The resulting shear boundary layers (SBLs) are likely to be an avenue for particle acceleration in relativistic jets. The effect of radiation drag on radiating particles has yet to be addressed in most studies of particle acceleration at shear boundary layers, even though radiative cooling may considerably affect particle dynamics. By using particle-in-cell simulations, we study the effects of inverse Compton cooling on particle dynamics and emerging particle spectra.

Keywords. shear boundary layers, shear acceleration, radiation mechanism, radiation-drag

1. Introduction

The relativistic jets emanating from the central engine of active galactic nuclei (AGNs) or gamma-ray bursts (GRBs) interact with ambient plasma resulting in jet stratification in the radial direction. In this picture, the jet is considered to consist of a fast-moving inner spine surrounded by a slow-moving outer sheath (e.g., Ghisellini et al. 2005). The resulting shear boundary layers (SBLs) are promising sites for particle acceleration in relativistic jets. Owen et al. (1989) first suggested the existence of radial stratification of the relativistic jets with velocity shear to explain the VLA radio observations of the M87 jet. Shear acceleration can be defined as a second-order-Fermi-type acceleration mechanism and is expected in fast, velocity-shearing plasma flows. SBLs in relativistic jets are subject to plasma instabilities like the Weibel instability (Weibel 1959), and two-stream instability (Boyd et al. 2003), which gives rise to the self-generation of electric and magnetic fields (e.g., Liang et al. 2013; Chand et al. 2019). The self-generated magnetic field develops the turbulence in SBLs from initially unmagnetized plasma, which eventually leads to particle acceleration (e.g., Alves et al. 2012; Liang et al. 2013). The particle acceleration in shear boundary layers has been broadly studied using PiC simulations due to its obvious astrophysical significance. However, most of these studies have overlooked the possible effect of radiation drag on particle dynamics.

The two prime radiative processes occurring at the SBLs of relativistic jets are synchrotron emission and inverse Compton (IC) emission due to the interaction of the relativistic electrons with the synchrotron photons (synchrotron self-Compton) or an external seed photon field (external Compton). We consider an inverse-Compton cooling of the relativistic electrons accelerated at SBLs due to the blackbody photon field in the Thomson regime. In particular, we investigate the effect of IC cooling on the particle

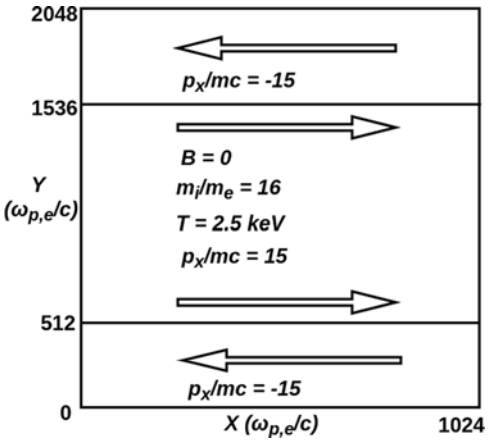

Figure 1. 2D simulation setup of the initially unmagnetized shear flow of the electron-ion plasma: the plasma consists of right-moving plasma (spine) in the central 50% of the Y-grid crammed between left-moving plasmas (sheath) occupying top 25% and bottom 25% of the Y-grid. Spine and sheath counterstream with equal and opposite x-momenta $p_x/mc = \pm 15$ in the ELF frame.

energy distribution at SBLs of relativistic jets. In section 2, we discuss our numerical model setup with the initial simulation parameters. In section 3, we describe a theoretical background of the IC cooling due a to blackbody target photon field and present the resulting particle spectra. We summarize our results in section 4.

2. Numerical Simulation Setup

We set up a 2D particle-in-cell (PiC) simulation of self-generation of B- and E- fields from initially unmagnetized plasma at SBLs in relativistic jets using the code TRISTAN-MP (Spitkovsky 2005). The dimension of the simulation boxes is 1024×2048 with shear boundary layers located at $Y = 512$ and $Y = 1536$ (see fig. 1). In the simulations, distances are measured in units of plasma skin depth (i.e., $\Delta x = c/\omega_{p,e}$), and time is measured in terms of inverse plasma frequency, ($\Delta t = 1/\omega_{p,e}$), where the plasma frequency is given by, $\omega_{p,e} = \sqrt{4\pi n e^2/m_e}$ (n, e, and m_e indicate electron density, electron charge, and electron mass, respectively), and c is the speed of light. The numerical speed of light is considered as $c = 0.45\Delta x/\Delta t$ to satisfy the Courant condition. We simulate 20 particles per cell with fiducial ion-to-electron mass ratio, $(m_i/m_e) = 16$. Our simulations are performed for pure electron-ion plasma. The upper and lower part of the simulation grid occupying 50 % of the box constitutes the sheath region, and the remaining central portion of the grid represents the spine region. The simulations are performed in equal Lorentz factor (ELF) frame of reference. The spine and sheath, with a uniform temperature of 2.5 keV, counterstream with an equal bulk Lorentz factor, $\Gamma = 15$.

3. Effect of Radiation Drag on Particle Spectra

The inverse Compton scattering of a single electron of Lorentz factor γ due to interaction with photons of energies $\varepsilon = h\nu/m_e c^2$ is described by the inverse Compton spectrum peaking at $\gamma^2\varepsilon$. We use a simple δ-function approximation with a characteristic photon frequency of $h\nu = 2.7 K_B T$ (K_B is the Boltzmann's constant) for the target photon field to calculate the inverse Compton cooling term. The radiation cooling term for inverse

https://doi.org/10.1017/S1743921323000637 Published online by Cambridge University Press

Compton scattering of relativistic electrons in the angle-integrated blackbody photon field in the Thomson regime and boosted to the spine frame is

$$\frac{d\gamma}{dt} = \Gamma_{rel}^2 \frac{\pi^4}{15} \sigma_T c K \gamma^2 \theta^4, \tag{1}$$

where $K = 8\pi/\lambda_C^3$, $\theta = K_B T/m_e c^2$, $\sigma_T = 8\pi e^4/3m_e^2 c^4$ is the Thomson cross section, and $\gamma = 1/\sqrt{1-\beta^2}$, with $\beta = v/c$ (v refers to the electron velocity). Here, λ_C, T, and e are Compton wavelength, radiation temperature, and electron charge, respectively. $\Gamma_{rel} = 2\Gamma^2 + 1$ is the relative bulk Lorentz factor between the spine and the sheath.

Considering the head-on collision between the electron and photons, the Compton cross section in the case of an angle-dependent target photon field can be approximated (Boettcher, Harris, & Krawczynski, 2012) as

$$\frac{d\sigma_C}{d\Omega_s d\varepsilon_s} = \frac{\pi r_e^2}{\gamma\varepsilon'} \left\{ y + \frac{1}{y} - \frac{2\varepsilon_s}{\gamma\varepsilon' y} + \left(\frac{\varepsilon_s}{\gamma\varepsilon' y}\right)^2 \right\} H\left(\varepsilon_s \; ; \; \frac{\varepsilon'}{2\gamma}, \; \frac{2\gamma\varepsilon'}{1+2\varepsilon'}\right), \tag{2}$$

where H is the Heaviside function that constrains the upper and lower limits of the scattered photon energies, and $y = 1 - \frac{\varepsilon_s}{\gamma}$. $\varepsilon' = \gamma\varepsilon(1-\beta\mu)$ is the initial photon energy in the electron's rest frame. $\mu = \cos\psi$, where ψ is the angle between the direction of propagation of the electron and photon. From equation (2), the Compton emissivity in the spine frame can be written as

$$\mathrm{j}(\varepsilon,\gamma,\mu) = \frac{3m_e c^3 \sigma_T \varepsilon_s \Gamma_{rel}^2 (1-\beta\mu)}{8\gamma} \int_0^\infty \frac{1}{\varepsilon'} \left\{ y + \frac{1}{y} - \frac{2\varepsilon_s}{\gamma\varepsilon' y} + \left(\frac{\varepsilon_s}{\gamma\varepsilon' y}\right)^2 \right\} n_{ph}(\varepsilon,\theta)$$
$$H\left(\varepsilon_s; \frac{\varepsilon'}{2\gamma}, \frac{2\gamma\varepsilon'}{1+2\varepsilon'}\right) d\varepsilon$$

With the δ-function approximation employed for the spectral calculation, the photon density is given by $n_{ph}(\varepsilon,\theta) = n_{ph}(\theta)\delta(\varepsilon - 2.7\theta)$. The photon density now simplifies to $n_{ph}(\theta) = 2.4K\theta^3$. After some simplifications, $\mathrm{j}(\varepsilon,\gamma,\mu)$ can be integrated over the scattered photon energy (ε_s) within the limits restricted by the Heaviside function (H) in equation (2) to get the cooling term for inverse Compton scattering (in both Thomson and Klein-Nishina regimes) of relativistic electrons in an angle-dependent photon field as

$$\frac{\mathrm{d}\gamma}{\mathrm{dt}}(\mu,\gamma,\theta) = A \left[\varepsilon_{s_{max}}^2 - \varepsilon_{s_{min}}^2 + \frac{\varepsilon_{s_{max}}^4 - \varepsilon_{s_{min}}^4}{4\gamma^2} + \frac{\varepsilon_{s_{max}}^5 - \varepsilon_{s_{min}}^5}{5\gamma^3} - \frac{2}{2.7\theta(1-\beta\mu)} \left\{ \frac{\varepsilon_{s_{max}}^3 - \varepsilon_{s_{min}}^3}{3\gamma^2} \right. \right. \tag{3}$$
$$\left. + \frac{\varepsilon_{s_{max}}^4 - \varepsilon_{s_{min}}^4}{4\gamma^3} \right\} + \frac{1}{\gamma^4} \frac{1}{(2.7\theta)^2(1-\beta\mu)^2} \left\{ \frac{\varepsilon_{s_{max}}^4 - \varepsilon_{s_{min}}^4}{4} + \frac{2\left(\varepsilon_{s_{max}}^5 - \varepsilon_{s_{min}}^5\right)}{5\gamma} \right.$$
$$\left. \left. + \frac{\varepsilon_{s_{max}}^6 - \varepsilon_{s_{min}}^6}{2\gamma^2} + \frac{4\left(\varepsilon_{s_{max}}^7 - \varepsilon_{s_{min}}^7\right)}{7\gamma^3} \right\} \right],$$

where $A \equiv \frac{0.3\Gamma_{rel}^2 \; c \; \sigma_T K\theta^2}{\gamma^2}$, $\varepsilon_{s_{max}} \equiv \frac{5.4\gamma^2(1-\beta\mu)\theta}{1+5.4\gamma\theta(1-\beta\mu)}$, $\varepsilon_{s_{min}} \equiv \frac{2.7\theta(1-\beta\mu)}{2}$ and $\mu \equiv \cos\psi$. ψ is the angle between the directions of propagation of the interacting photon and electron.

Figure 2 demonstrates the effect of IC cooling on electron spectra due to UV photons (i.e., $\theta = 10^{-5}$). The electron spectra evolve from an initial Maxwellian to non-Maxwellian plus a remnant of the initial Maxwellian spectra. At steady state, the spectra peak at around $\gamma \cong \Gamma \mathrm{m_i}/\mathrm{m_e}$. The IC cooling depends on the radiation density and the Lorentz factor of electrons. At lower electron energies, the effect of the cooling is almost non-existent.

https://doi.org/10.1017/S1743921323000637 Published online by Cambridge University Press

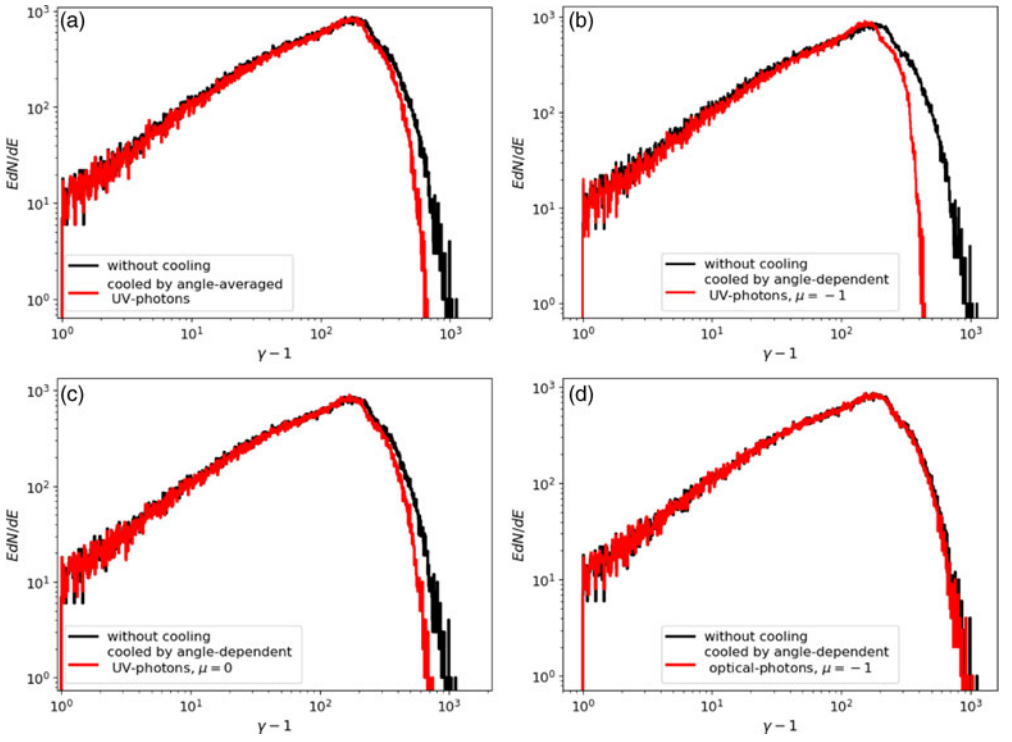

Figure 2. Comparison of Particle spectra with and without IC cooling due to UV-photons (panels a, b, and, c), and optical photons (panel d): spectra are produced at $t = 3000/\omega_{p,e}$.

However, IC cooling strongly affects electron acceleration and the electron energy spectrum at higher energies. As a result of radiation drag, the high-energy end of the spectrum shifts towards low-energies (see fig. 2). Unlike the IC cooling due to UV photons, the IC cooling strength for photons with temperature $\theta \leq 10^{-6}$ is highly subdominant. As a result, the particle dynamics and the electron energy spectrum are not appreciably affected by Compton drag.

4. Conclusion

In this paper, we discussed the results of two-dimensional PiC simulations of pure electron-ion plasmas at SBLs in relativistic jets with no initial magnetic fields, subject to IC cooling. We considered both angle-averaged and angle-dependent distribution of target photons with a δ-function approximation employed for the target photon field. We demonstrated that the relativistic particles accelerated at SBLs in relativistic jets may be substantially affected due to IC cooling. Due to the strong IC losses, high-energy electrons get cooled down to slightly lower energies. The effect of IC cooling is significantly high for the inverse Compton scattering by relativistic electrons off blackbody photons of higher temperatures (i.e., $\theta \geq 10^{-6}$). However, the highest energy end of the spectrum is slightly shifted toward lower energies. The particle spectrum is roughly unchanged for the lower temperatures of target photons (i.e., $\theta < 10^{-6}$). In the future, it may also be useful to investigate how the results change if we adopt an electron-proton plasma with a non-zero magnetic field at SBLs in relativistic jets.

https://doi.org/10.1017/S1743921323000637 Published online by Cambridge University Press

Acknowledgments

This work is supported through the South African Research Chair Initiative (SARChI) of the Department of Science and Technology and the National Research Foundation† (NRF) of South Africa under SARChI chair grant no. 64789.

References

Alves, E. P., Grismayer, T., Martins, S. F., et al. 2012, The Astrophysical Journal Letters, 746, L14, doi: 10.1088/2041-8205/746/2/L14

Boettcher, M., Harris, D.E., & Krawczynski H.: 2012, Relativistic Jets from Active Galactic Nuclei

Boyd, T. M., Boyd, T., & Sanderson, J. 2003, The physics of plasmas (Cambridge university press)

Chand, T. B., Böttcher, M., & Kilian, P. 2019, PoS, HEASA2018, 046

Ghisellini, G., Tavecchio, F., & Chiaberge, M. 2005, A&A, 432, 401, doi: 10.1051/0004-6361: 2004140410.48550/arXiv.astro-ph/0406093

Liang, E., Boettcher, M., & Smith, I. 2013, The Astrophysical Journal, 766, L19

Liang, E., Fu, W., Boettcher, M., Smith, I., & Roustazadeh, P. 2013, The Astrophysical Journal Letters, 779, L27, doi: 10.1088/2041-8205/779/2/L27

Owen, F. N., Hardee, P. E., & Cornwell, T. J. 1989, ApJ, 340, 698, doi: 10.1086/167430

Spitkovsky, A. 2005, AIP Conference Proceedings, doi: 10.1063/1.2141897

Weibel, E. S. 1959, Phys. Rev. Lett., 2, 83, doi: 10.1103/PhysRevLett.2.83

† Any opinion, finding and conclusion, or recommendation expressed in this material is that of the authors, and the NRF does not accept any liability in this regard.